

Synthesis of MnWO_4 nanorods and its electrical and electrochemical properties

S. Saranya · S. T. Senthilkumar · K. Vijaya Sankar ·
R. Kalai Selvan

Received: 22 September 2011 / Accepted: 9 March 2012 / Published online: 21 March 2012
© Springer Science+Business Media, LLC 2012

Abstract The MnWO_4 nanorods were successfully synthesized by surfactant assisted ultrasonics method and characterized its structural (XRD), morphological (SEM) electrical (solid state impedance) and electrochemical (CV) properties. The X-ray diffraction patterns inferred the formation of highly crystalline monoclinic structure of MnWO_4 . The formation of nanorods with the aspect ratios of 30–40 nm were reveals from SEM image. The maximum d.c. electrical conductivity was found to be 4.40×10^{-5} S/cm at 570°C for MnWO_4 nanorods prepared by surfactant assisted ultrasonic method. The quasi-rectangular behavior of cyclic voltammogram inferred the supercapacitive behavior of the prepared MnWO_4 nanorods.

Keywords Metal tungstates · X-ray diffraction · Nanocrystalline materials · Electrical conductivity

1 Introduction

Nowadays, there is much interest on the synthesis of nanostructured materials due to their unusual properties which are differ from their bulk materials. In nanomaterials, the electronic states, defects and surface chemistry are selectively tunable by varying the synthesis conditions. This induced the fabrication of variety of metallic, organic, inorganic and hybrid nanomaterials for versatile applications. Among the mixed metal oxides, the ABO_4 type wolframite structures received prominent interest due to their versatile properties

in various potential applications. This wolframite structures is made up of hexagonally closed packed oxygens with octahedral sites filled by A and B cations in a regular manner [1]. Especially, MnWO_4 has huebnerite structure, which is a member of wolframite structure having numerous applications including luminescent [2], sensors [3], optical fibres and scintillator materials [4]. In MnWO_4 , each Mn and W atoms are in octahedral coordination surrounded by six nearest neighbour oxygen atoms. It consists of a number of edge-sharing (MnO_6) and (WO_6) octahedrons in a series of zigzags along c-axis. The oxygen ions are hexagonally closed packed and the metal ions occupy a quarter of all the octahedral interstices. Mn and W atoms are alternatively arranged parallel to the (100) planes [5]

MnWO_4 nanostructures have been prepared by sol–gel method [6], chemical reaction in molten salt media [7] and high temperature decomposition of complex precursors [8]. Now there are various synthesis methods available for the preparation of MnWO_4 nanostructures such as nanowires by template synthesis [9], nanofibers and nanorods by surfactant assisted complexation-precipitation method [10], nanoplates by hydrothermal method [11], nanococoons [12] and nanoflowers [13] by solvothermal method and cyclic microwave assisted spray synthesis [14] and spray pyrolysis method [15]. In the present work, we have prepared MnWO_4 nanorods by surfactant assisted ultrasonics synthesis and studied their electrical and electrochemical properties. The main aim of this study is to explore the prepared MnWO_4 as an active electrode material for supercapacitor applications.

2 Experimental

The MnWO_4 nanorods were synthesized by co-precipitation method using $\text{MnCl}_2 \cdot 4\text{H}_2\text{O}$ and $\text{Na}_2\text{WO}_4 \cdot 2\text{H}_2\text{O}$ as the

S. Saranya · S. T. Senthilkumar · K. V. Sankar · R. K. Selvan (✉)
Solid state Ionics and Energy Devices Laboratory,
Department of Physics, Bharathiar University,
Coimbatore 641 046, India
e-mail: selvankram@buc.edu.in

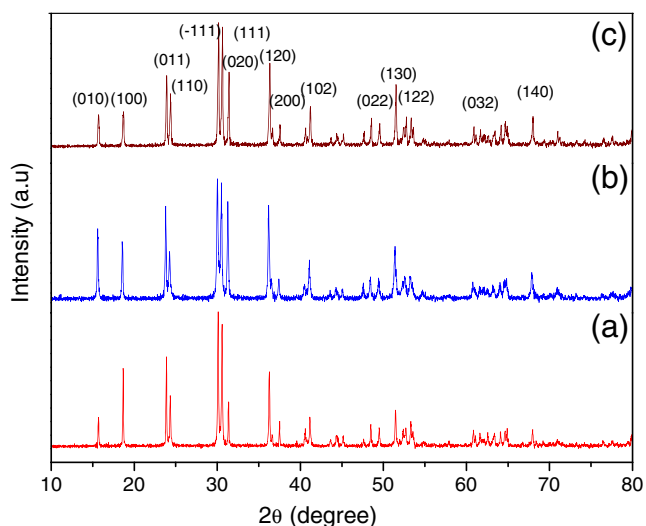


Fig. 1 XRD pattern of (a) MnWO₄-A, (b) MnWO₄-B and (c) MnWO₄-C

starting precursors. Stoichiometric quantities of starting compounds were dissolved in desired amount of distilled water individually and Na₂WO₄·2H₂O solution was added drop wise to MnCl₂·4H₂O solution under constant mechanical stirring for an hour. The resulting mixture was centrifuged and washed several times with distilled water to remove the impurities. Further the precipitate was collected and dried at 100°C for 2 h and finely ground. The same procedure was repeated to prepare MnWO₄ nanorods under ultrasonication. Similarly, to study the effect of surfactants on the synthesis of MnWO₄, 0.001 mol of cetyl trimethyl ammonium bromide (CTAB) was used as the soft template. The MnWO₄ nanoparticles prepared by simple co-precipitation, ultrasonication and surfactant (CTAB) assisted ultrasonication method is denoted hereafter as MnWO₄-A, MnWO₄-B and MnWO₄-C, respectively.

To increase the crystallinity of the materials, the powders were further calcined at 800°C for 5 h. The x-ray diffraction pattern of the tungstates was measured with a Bruker AXS D8 Advance powder x-ray diffractometer (Cu Kα=1.5418 Å). The lattice parameter values are calculated using CELREF software. The particle morphology and structure were studied with transmission electron microscopy on a JEOL-JEM 100 SX TEM microscope, working at 80 kV accelerating voltage. Impedance and conductance studies were

carried out on a HIOKI 3532 LCR HITESTER in the frequency range of 42 Hz–4 MHz. For better ohmic contact silver paste was applied to both surfaces of the pellet, before being sandwiched between the two electrodes of sample holder. For the electrode preparation, 80% of active material 10% conductive carbon black and 10% of PVDF (polyvinylidene fluoride) was blended well in the solvent N-methyl-2-pyrrolidone (NMP) to obtain a homogeneous mixture. The slurry (1 mg) was coated on the carbon electrode (1 cm²) for the electrochemical studies. The electrochemical analysis such as cyclic voltammetry and galvanostatic charge/discharge analysis were carried in three electrode systems using Bio Logic (SP 150) electrochemical work station. Here, a platinum electrode and a saturated Ag/AgCl electrode were used as counter and reference electrodes, respectively.

3 Results and discussion

The crystalline structure, phase purity and grain size of MnWO₄ is enumerated from the X ray diffraction studies. The XRD pattern of 800°C calcined MnWO₄-A, MnWO₄-B and MnWO₄-C nanoparticles are shown in Fig. 1(a–c) and the calculated structural parameters are given in Table 1. The diffraction pattern (Fig. 1(a)) of MnWO₄ synthesized through co-precipitation method (MnWO₄-A), consisted of peaks at 2θ=15.70, 18.66, 23.88, 24.34, 30.10, 30.57, 31.35, 36.25, 37.50, 41.15, 48.46, 51.47, 52.70, 60.85 and 67.97 corresponding to the planes of (010), (100), (011), (110), (–111), (111), (020), (120), (200), (102), (022), (130), (122), (032) and (140) respectively. The calculated lattice parameters a=4.7982 Å, b=5.7478 Å, c=4.9801 Å, α=90°, β=91.3286°, γ=90° enumerate the monoclinic structure. The average grain size of 71 nm is obtained using Debye Scherrer formula. XRD peaks of both the MnWO₄-B (Fig. 2(b)) and MnWO₄-C (Fig. 2(c)) have the same lattice planes and the calculated lattice parameters are a=4.8122 Å, b=5.7545 Å, c=4.9847 Å, α=90°, β=91.1197°, γ=90° with a grain size of 65 nm and a=4.7960 Å, b=5.7457 Å, c=4.9802 Å, α=90°, β=91.1409°, γ=90° with the grain size of 75 nm. All the calculated structural parameters are matched well with the

Table 1 Structural parameters

Sample	Lattice parameters				V (Å ³)	D, g/cm ³	Grain size, nm
	a (Å)	b (Å)	c (Å)	β			
MnWO ₄ -A	4.798	5.747	4.980	91.32°	137.3	388.4	71
MnWO ₄ -B	4.812	5.747	4.984	91.11°	138.0	382.5	65
MnWO ₄ -C	4.796	5.745	4.980	91.14°	137.2	389.2	75

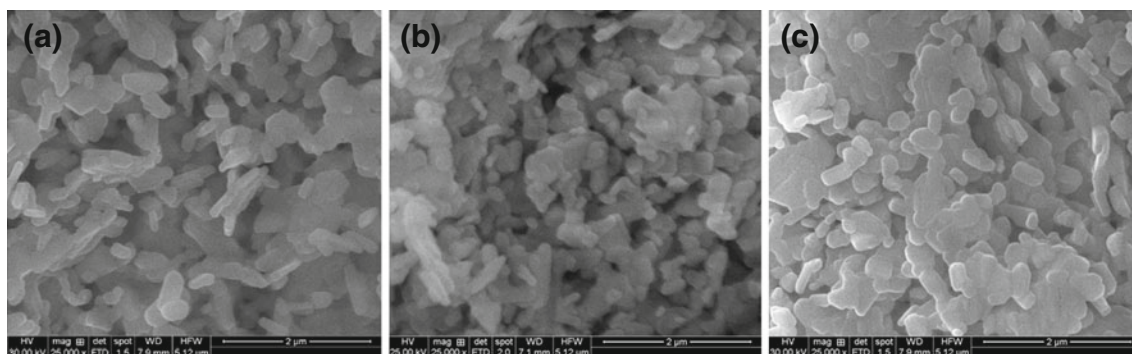


Fig. 2 SEM images of (a) $\text{MnWO}_4\text{-A}$, (b) $\text{MnWO}_4\text{-B}$ and (c) $\text{MnWO}_4\text{-C}$

JCPDS (72-0478) values. The lattice parameters determined from the XRD pattern enumerated that MnWO_4 has monoclinic structure with P2/C space group.

The morphological features of the samples are identified by SEM images and are shown in Fig. 2. The SEM image of $\text{MnWO}_4\text{-A}$ is shown in Fig. 2(a). It shows that the particles are uniformly distributed and have a rod like structure. The diameter of the individual nanorods is ~ 100 nm and the length is 400 nm. Maximum number of rods exists with 100–125 nm in diameter and 250–300 nm in length. The size of the MnWO_4 nanorods by ultrasonication method ($\text{MnWO}_4\text{-B}$) is about ~ 500 nm in length and ~ 100 nm in dia. Maximum number of particles lie in the range of 100–125 nm diameters and 200–300 nm length (Fig. 2(b)). Figure 2(c) denotes the SEM images of $\text{MnWO}_4\text{-C}$. These nanorods have the diameter of about 20–200 nm and length of 100–550 nm. The rods obtained in co-precipitation method looks longer than other methods.

In ultrasonication method, the acoustic vibration may break the growth of rods, while in surfactant assisted sonication method the one dimensional growth of nanorod may be inhibited by CTAB.

Figure 3 (a and b) shows the cole–cole plot (Z' vs Z'') of $\text{MnWO}_4\text{-B}$ and $\text{MnWO}_4\text{-C}$ measured in the temperature range of 510–570°C. The calculated impedance parameters of MnWO_4 are given in Table 2. The spectra contain a single semicircle representing the parallel combination of resistance and capacitance at high frequencies and grain

boundary effects at low frequencies [16]. The semicircle depends on the strength of relaxation and the available frequency range. The radius of the semicircle decreases with increasing temperature, which means that the semicircle gets depressed along real axis. This indicates the presence of a distribution of relaxation process [17] within the bulk response or some grain boundary relaxation. The intercept of the semicircle with real axis gives the bulk resistance (R_b) value of the sample. The bulk conductivity can be calculated using ' R_b ' value from the formula, $\sigma_b = l/R_b A$, S/cm, where l is the thickness of the pellet, A is the contact area of the pellet. While increasing the temperature, the resistance decreases which results in the raising of conductivity, due to the thermally activated charge carriers. This enumerates the negative temperature coefficient of resistance or semiconducting nature of the sample [18]. The activation energy required for the hopping of charge carriers can be found from the Arrhenius relation, $\sigma(T) = \sigma_0 \exp(E_a/kT)$. From the Arrhenius plot the value of E_a is 0.621 eV for MnWO_4 obtained via ultrasonication and 0.325 eV for $\text{MnWO}_4\text{-C}$ through surfactant assisted ultrasonication. The bulk capacitance can be determined at the maximum frequency using the relation $2\pi\gamma_{\max}RC = 1$, is in the range of pico farad and reveals that the conduction process through the bulk of the material. The maximum conductivity at 570°C was found to be 4.23×10^{-5} S/cm for $\text{MnWO}_4\text{-C}$ and 1.186×10^{-6} S/cm for $\text{MnWO}_4\text{-B}$.

The conductivity spectra of MnWO_4 prepared in ultrasonication and surfactant assisted ultrasonication method are

Fig. 3 Solid state impedance spectra of (a) $\text{MnWO}_4\text{-B}$ and (b) $\text{MnWO}_4\text{-C}$

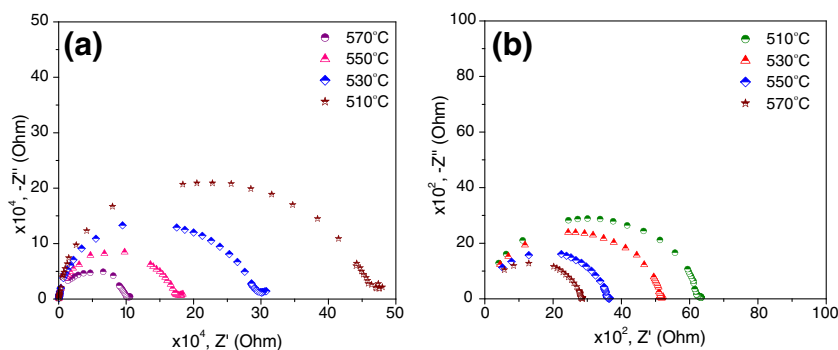


Table 2 Impedance parameters of MnWO₄

Temp. °C	MnWO ₄ -B			MnWO ₄ -C		
	R _b (Ω), × 10 ⁴	C _b (pF)	σ _b × 10 ⁻⁷ (S/cm)	R _b (Ω) × 10 ³	C _b (pF)	σ _b × 10 ⁻⁵ (S/cm)
510	4.752	47.86	2.58	6.359	35.7	1.98
530	3.039	52.38	4.04	5.249	33.7	2.40
550	1.795	88.68	7.02	3.667	43.4	3.44
570	1.035	51.25	11.8	2.983	26.6	4.23

shown in Fig. 4 (a and b). The values of d.c. conductivity (σ_{dc}), hopping frequency (ω_p) and mobility (μ) of the samples are given in Table 3. This gives prominent information related to the transport of charge carriers that is involved in the conduction process and their behavior as a function of temperature and frequency. The low frequency plateau corresponds to the dc conductivity of the bulk and the high frequency dispersive region corresponds to the ac conductivity [19]. Usually, the conducting mechanism in solids is analyzed by Jonscher’s universal power law and

the conductivity plot is fitted on the basis of this law, which relates σ(ω)=σ_o+Aωⁿ. Where, σ (ω) is the ac conductivity, σ_o is d.c conductivity, A is the temperature dependent parameter and is the temperature dependent exponent. The value of ‘A’ determines the polarization strength and ‘n’ represents the degree of interaction between the mobile ions and the lattices. When ‘n’ is lesser than 1 hopping is due to the translation motion and when n >1, the motion involves the charges without leaving the neighborhood [20]. In the MnWO₄ conduction mechanism, the value of ‘n’ is greater than 1 for all the temperatures. The maximum conductivity is determined as 1.21 × 10⁻⁶ S/cm for ultrasonication and 4.40 × 10⁻⁵ S/cm for surfactant assisted ultrasonication method at 570°C. The conductivity increases with raise in temperature due to the movement of thermally activated ions from one site to another and also due to the creation of defects [21]. The hopping frequency (ω_p), where the change in conductive region from low to high frequency dispersion occurs, corresponds to the hopping of charge carriers. The value of ω_p and also the mobility of charge carriers increases with temperature because the charges accumulated at the grain boundaries gain sufficient energy to jump over the barrier. This suggests that conduction mechanism due to the hopping of charge carriers. From both the impedance and conductance spectrum, the electrical conductivity is high for MnWO₄ synthesized under surfactant assisted ultrasonication using CTAB. This can be explained based on the grain size of the particles. The grain size of MnWO₄ prepared with and without CTAB are 75 nm and 65 nm respectively. The decrease in conductivity on the reduction in grain size may be caused by the size effects. The increase in grain boundary volume associated with the impedance to the flow of carriers may also be

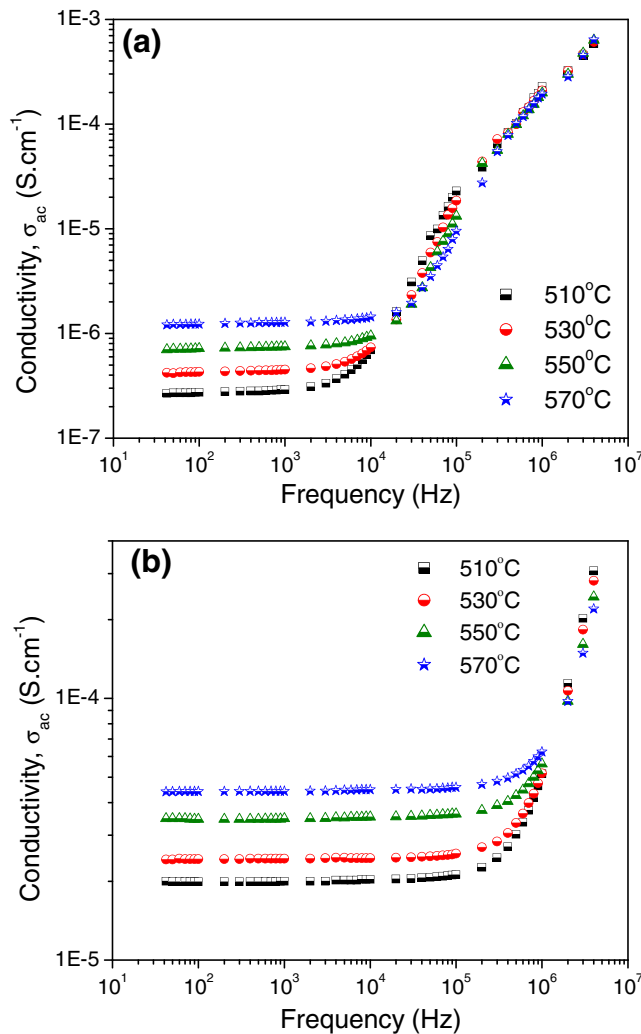


Fig. 4 Conductance spectra of (a) MnWO₄-B and (b) MnWO₄-C

Table 3 Conductance parameters of MnWO₄

Temp. °C	MnWO ₄ -B			MnWO ₄ -C		
	σ _{dc} × 10 ⁻⁷ (S/cm)	ω _p (Hz) × 10 ³	μ × 10 ¹⁹	σ _{dc} (S/cm) × 10 ⁻⁵	ω _p (Hz) × 10 ⁵	μ × 10 ²¹
510	2.68	07.33	05.85	2.00	07.64	06.105
530	4.21	10.60	08.25	2.42	09.17	08.643
550	7.01	17.53	13.34	3.47	12.63	09.616
570	12.10	31.73	23.53	4.40	16.83	12.481

responsible for this behavior. Also, the activation energy required for the grain boundary conduction is high for small grain size. The decrease in conductivity with increase in activation energy resembles the blocking nature of the grain boundary. The hopping frequency also shifts to lower values with the decrease in grain size which will further reduce the mobility of the charge carriers and also the conductivity [22, 23].

The representative cyclic voltammogram of $\text{MnWO}_4\text{-C}$ are shown in Fig. 5 at various scan rates. There is no significant oxidation/reduction peaks were observed and quasi-rectangular shape of the curve attributes to the non-faradic/electrical double layer charge storage process of MnWO_4 . The calculated specific capacitance (SC) values of MnWO_4 is 27, 23, 18, 16, 15, 13 and 12 F/g corresponding to the various scan rates of 5, 10, 20, 30, 40, 50, 100 and 200 mV/s respectively. It can be seen that the SC values were decreased with increase in scan rate reveals that the minimum utilization of bulk of the active material. The observed SC values are less when compare with the reported values of WO_3 and MnO_2 . The SC of the MnWO_4 can be further improved by coating with carbon or making composite with conducting polymers.

Figure 6 shows the galvanostatic charge–discharge curves of MnWO_4 at 1 M H_2SO_4 electrolyte in the potential range between 0 and 1.2 V measured at different current densities of 1.3, 1.5, 2, 2.3 and 2.5 mA/cm^2 . It can be seen that the charge–discharge curves are almost symmetrical in nature, which reveals the high reversibility nature of MnWO_4 electrodes. However, a small IR or potential drop was found at the discharge curve [24, 25]. The calculated specific capacitance values are 16, 15, 13, 11 and 9 Fg^{-1} at various current densities of 1.3, 1.5, 2.0, 2.3 and 2.5 mA/cm^2 respectively. The high specific capacitance values are obtained at low current density than at higher current density. It is well known that at low current density the ions from the electrolyte can utilize all the available sites in the inner and outer surface of the electrode material that leads to the higher capacitance and vice versa. The cyclic stability of MnWO_4 electrode was

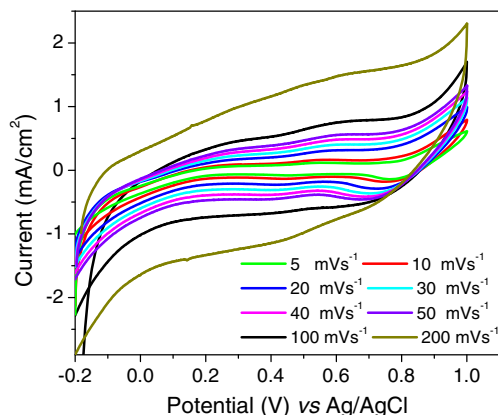


Fig. 5 Cyclic voltammogram of $\text{MnWO}_4\text{-C}$

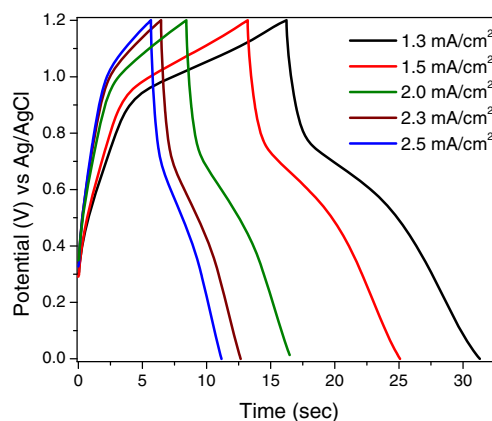


Fig. 6 Galvanostatic charge–discharge curve of $\text{MnWO}_4\text{-C}$ at different current densities

investigated using 1 M H_2SO_4 electrolyte at the current density of 2 mA/cm^2 up to 1,000 cycles. Figure 7 shows the calculated specific capacitance and coulombic efficiency of the electrodes with respect to cycle number. It shows that the specific capacitance of MnWO_4 electrode gets increased from 12.5 Fg^{-1} to 25 Fg^{-1} while increasing the cycle number. This enhancing specific capacitance during cycling may be due to morphological or phase changes occurred in the electrode material. The similar type of reports already was reported in elsewhere [26].

4 Conclusion

MnWO_4 nanorods were successfully synthesized by simple co-precipitation, ultrasonication and surfactant assisted ultrasonication method. The structural parameters determined from X-ray diffraction studies confirmed the monoclinic structure of MnWO_4 . The morphology of MnWO_4 nanorods, were revealed by SEM images. The conductivity of MnWO_4 prepared through surfactant assisted ultrasonication method was 4.23×10^{-5} S/cm and through ultrasonication method was

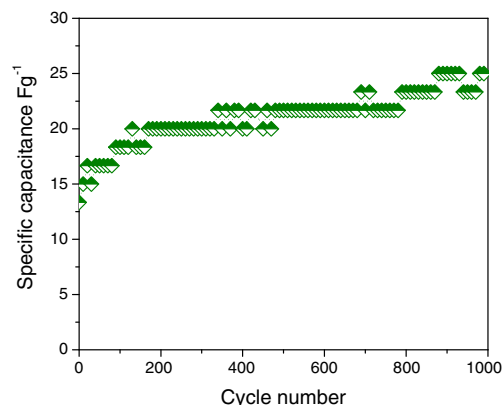


Fig. 7 Cyclic stability of $\text{MnWO}_4\text{-C}$ at constant current density of 2 mA/cm^2

1.186×10^{-6} S/cm at 570°C. The conductivity increases with increase in temperature confirmed the semiconducting nature of the material. The high conductivity was obtained for surfactant assisted ultrasonication method as CTAB produced MnWO₄ with large grain size. The CV and charge–discharge studies performance confirmed the capacitance behavior of MnWO₄ nanorods.

References

1. A.W. Sleight, *Acta Cryst.* **B28**, 2899 (1972)
2. H.D. Nguyen, D. Mrabet, T.T.D. Vu, C.T. Dinh, T.O. Do, *Cryst Eng Comm.* **13**, 1450 (2011)
3. A.M.E.S. Raj, C. Mallika, O.M. Sreedharan, K.S. Nagaraja, *Mater. Lett.* **53**, 316 (2002)
4. S.H. Yu, B. Liu, M.S. Mo, J.H. Huang, X.M. Liu, Y.T. Qian *Adv. Funct. Mater.* **13**, 639 (2003)
5. O. Heyer, N. Hollmann, I. Klassen, S. Jodlauk, L. Bohaty, P. Becker, J.A. Mydosh, T. Lorenz, D. Khomskii, *J. Phys. Condens. Matter.* **18**, L471 (2006)
6. W. Qu, W. Wlodarski, J.U. Meyer, *J. Sensors Actuat. B* **64**, 76 (2000)
7. D. Schultze, K.T. Wilke, C. Waligora, *Z. Anorg. Allg. Chem.* **352**, 184 (1976)
8. M. Jang, T.J.R. Weakley, K.M. Doxsee, *Chem. Mater.* **13**, 519 (2001)
9. H. Zhou, Y. Yiu, M.C. Aronson, S.S. Wong, *J. Solid State Chem.* **181**, 1539 (2008)
10. S. Lei, K. Tang, Z. Fang, Y. Huang, H. Zheng, *J. Nanotech.* **16**, 2407 (2005)
11. L. Zhang, C. Lu, Y. Wang, Y. Cheng, *Mater. Chem. Phys.* **103**, 433 (2007)
12. W.B. Hu, X.L. Nie, Y.Zh. Mi, *Mater. Charact.* **61**, 85 (2010)
13. Y. Xing, S. Song, J. Feng, Y. Lei, M. Li, H. Zhang, *Solid State Sci.* **10**, 1299 (2008)
14. S. Thongtem, S. Wannapop, A. Phuruangrat, T. Thongtem, *Mater. Lett.* **63**, 833 (2009)
15. S. Thongtem, S. Wannapop, T. Thongtem, *Trans. Nonferrous. Met. Soc. China* **19**, s100 (2009)
16. A. Shukla, R.N.P. Choudary, A.K. Thakur, D.K. Pradhan, *Physica B* **405**, 99 (2010)
17. R. Rajan, R. Kumar, B. Behera, R.N.P. Choudary, *Physica B* **404**, 3709 (2009)
18. A. Kumar, B.P. Singh, R.N.P. Choudary, A.K. Thakur, *J. Alloys Compd* **394**, 292 (2005)
19. M. Ram, *Solid State Sci.* **12**, 350 (2010)
20. B. Behera, P. Nayak, R.N.P. Choudary, *J. Alloys Compd* **436**, 226 (2007)
21. Y. Yadav, M.P.K. Sahoo, R.N.P. Choudary, *J. Alloys Compd* **490**, 589 (2010)
22. N. Ponpandian, P. Balaya, A. Narayanasamy, *J. Phys. Condens. Matter.* **14**, 3221 (2002)
23. A. Chandra Bose, P. Balaya, P. Thangadurai, S. Ramasamy, *J. Phys. Chem. Solids* **64**, 659 (2003)
24. J. Xu, L. Gao, J. Cao, W. Wang, Z. Chen, *Electrochim. Acta* **56**, 732 (2010)
25. J. Zhang, J. Jiang, X.S. Zhao, *J. Phys. Chem. C* **115**, 6448 (2011)
26. D.P. Dubal, D.S. Dhawale, R.R. Salunkhe, C.D. Lokhande, *J. Alloys Compd.* **496**, 370 (2010)